Am J Transl Res 2017;9(5):2579-2594
www.ajtr.org /ISSN:1943-8141/AJTR0045223

*Original Article*

# Fat tissue, a potential Schwann cell reservoir: isolation and identification of adipose-derived Schwann cells

Lulu Chen[1,2*], Yuqing Jin[2*], Xiaonan Yang[1], Zhangyin Liu[2], Yang Wang[2], Gangyang Wang[2], Zuoliang Qi[1], Zunli Shen[2]

*[1]Department No. 16 of Plastic Surgery Hospital, Chinese Academy of Medical Sciences & Peking Union Medical College, Beijing, PR China; [2]Department of Plastic and Reconstructive Surgery, Shanghai 1st People's Hospital, Shanghai Jiao Tong University School of Medicine, Shanghai, PR China. [*]Equal contributors.*

Received November 27, 2016; Accepted February 6, 2017; Epub May 15, 2017; Published May 30, 2017

**Abstract:** Schwann cells can be used to promote peripheral nerve repair. However, it is challenging to obtain abundant autologous Schwann cells without sacrificing nerve integrity. In this study, we isolated Schwann cells from murine inguinal adipose tissue and identified the cell phenotype and function in vivo and in vitro. Through H&E and immunofluorescence staining, we detected tiny nerve fibers and Schwann cells in adipose tissue. We evaluated the phenotype of spindle-shaped cells (Schwann cell-like cells, SCLCs) isolated from adipose tissue using immunofluorescence staining and real-time RT-PCR. The results showed that SCLCs expressed specific Schwann cell markers. Analysis of conditioned SCLC culture media showed that, similar to Schwann cells isolated from sciatic nerves, SCLCs secreted NGF and BDNF. SCLCs were harvested from CAG-EGFP transgenic mice and combined with silicone nerve conduits to repair sciatic nerve defects in wild-type mice. Six months post-surgery, we found EGFP-positive SCLCs forming myelin sheaths in the same way as sciatic nerve-derived Schwann cells. This research indicates the existence of Schwann cells in adipose tissue and identifies the spindle-shaped cells isolated from adipose tissue as Schwann cells using in vitro and in vivo evaluations. Thus, SCLCs might be promising seed cells for peripheral nerve tissue engineering.

**Keywords:** Schwann cells, adipose tissue, isolation and identification of adipose-derived Schwann cells

## Introduction

Schwann cells (SCs) are seed cells for the nerve tissue regeneration which play an important role in peripheral nerve regeneration [1, 2]. SCs secrete various extracellular matrix components and nerve growth factors to promote axonal regeneration [3, 4]. In the Wallerian degeneration process after axon damage, SCs dedifferentiate, proliferate, remove myelin debris, and form Bungner bands to guide axon regeneration [5].

Two main sources for collecting autologous SCs include autologous nerve segments [6, 7], such as the sural nerve which can be surgically removed, and stem cells, such as bone marrow mesenchymal stem cells [8], hair follicle stem cells [9], and skin-derived precursors [10, 11]. However, autologous nerve segment donor sites are very limited and can result in sensory or motor function disorders in the donor areas [12, 13]. Although the number of stem cells in animal is high, there are still various problems in applying the cells, including low induction rate, long induction period, complicated induction steps, unstable differentiation results [14, 15], and the possibility of tumorigenicity [16]. Thus, it's badly needed to explore new source of Schwann cells.

In the clinic, patients who undergo liposuction often report numbness in the liposuction areas immediately after surgery, which gradually recovers within several weeks to months postoperatively [17, 18]. Thus, we speculated that this phenomenon was mainly caused by subcutaneous adipose tissue nerve damage and regeneration. In addition, many studies have also demonstrated that adipose tissue contains various cell components [19] and autonomic nerves [20-23]. Since nerve fibers are

found in adipose tissue, it is possible to collect SCs from adipose tissue.

To test our hypothesis, we isolated SCs in mouse inguinal adipose tissue and identified the cell phenotype and function both in vivo and in vitro.

## Materials and methods

### *Experimental animals*

Thirty C57BL/6-Tg (CAG-EGFP) C14-Y01-FM13-10sb mice aged between 5 and 7 days (CAG-EGFP mice; Model Animal Research Center of Nanjing University, Nanjing, China) and 30 age-matched C57BL/6J mice (WT mice; Shanghai SLAC Laboratory Animal Co., Ltd., Shanghai, China) were sacrificed to acquire sciatic nerves and inguinal adipose tissues. Spindle-shaped cells isolated from sciatic nerve tissue were designated SNSCs. Cells exhibiting fibroblast morphology isolated from adipose tissue were designated FLCs. Spindle-shaped cells isolated from adipose tissue were designated SCLCs. Another thirty-two eight-week-old WT mice (aged 8 weeks) were randomly divided into four groups as recipients for the in vivo study.

All animal experiment protocols were approved by the Animal Experiment and Care Committee of Shanghai Jiao Tong University School of Medicine. The methods were carried out in accordance with the relevant guidelines, including any relevant details.

### *Cell isolation, culture and purification*

Cells were isolated, cultured and purified according to previously reported protocols [24, 25]. We carefully dissected sciatic nerve segments (8-10 mm in length) or inguinal adipose tissues under a dissecting microscope. The segments were temporarily conserved in a 50 ml conical centrifuge tube (BD Falcon, USA) containing 10 ml DMEM (Gibco, Canada) supplemented with 10% fetal bovine serum (FBS; Hyclone, Australia).

Tissues were placed in a 50 ml conical centrifuge tube containing an enzymatic solution (50 μl per segment) prepared by dissolving Collagenase NB4 (Serva, Germany) and DispaseII (Serva) into DMEM at a concentration of 0.2% (0.27 U/ml). The tissue segments were incubated within a cell oscillator (Thermo, USA) at 37°C for 60 min until the tissues were entirely dissolved. The solution was centrifuged at 600×g for 5 min. After removing the supernatant, the cell pellets were resuspended in Schwann cell culture media (SCCM) composed of DMEM medium supplemented with 10% FBS, 2 μM forskolin (Sigma, USA) and 10 ng/ml heregulin-β-1 (Pepro Tech, USA) [24]. The cell suspensions were then added to a flask at a density of 2.0-2.5×$10^4$ cells per $cm^2$ and incubated at 37°C in a humidified atmosphere containing 5% carbon dioxide.

After 48 h of sciatic nerve cell cultivation or 24 h of adipose tissue cell cultivation, we replaced the culture media with 0.2% DispaseII diluted in DMEM with a volume of 0.1 ml/$cm^2$. After incubating at 37°C for 10-15 min, some cells were in suspension (i.e. SCLCs or SNSCs), while the rest remained adhered to flask (i.e. FLCs). The suspended cells were collected into a 15 ml conical tube (BD Falcon, USA) and centrifuged at 600×g for 5 min. After removing the supernatant, the pellet was suspended in SCCM and added to a flask at a density of 2.0-2.5×$10^4$ cells/$cm^2$. After 48 h of cultivation, cells were purified with 0.2% DispaseII and then resuspended in SCCM for further 48 h cultivation. At the same time, adherent adipose-derived primary cells (i.e. FLCs) were cultured in SCCM to passage 2 for 48 h cultivation.

Six cell photos of 100× magnification were randomly chosen to calculate the percent positive cells as follows: SCLCs purity = spindle-shaped cells/total adherent cells; Percent $Sox10^+$ SCLCs (i.e. SCs purity) = $Sox10^+$ spindle-shaped cells/total adherent cells; percent $Sox10^+$ cells = $Sox10^+$ spindle-shaped cells/total spindle-shaped cells (SCLCs or SNSCs); percent $S100^+$ cells = ($S100^+$ spindle-shaped cells/total spindle-shaped cells)×percent $Sox10^+$ cells. Computational methods for calculation of the percent $P75^{NTR+}$ cells, $NCAM^+$ cells and $MBP^+$ cells were the same as $S100^+$ cells

### *Immunofluorescent staining*

*Cell samples:* Cells were fixed with 4% paraformaldehyde (PFA) for 20 min, washed with PBS three times, and then blocked with 10% goat serum diluted in 0.5% bovine serum album (Sigma, USA) for 30 min at room temperature. After washing in PBS, cells were incubated with rabbit anti-$P75^{NTR}$ (1:500 diluted in PBS; Abcam,

Cambridge, UK), anti-S100 (1:500; Dako, Glostrup, Denmark), anti-NCAM (1:500; Millipore, Billerica, MA, USA), anti-MBP (1:100; Abcam), and anti-Sox10 (1:100; Abcam,) at 37°C for 1 h. After washing three times with PBS, cells were incubated with Alexa Fluor 555 goat anti-rabbit IgG (1:1000; Invitrogen, Carlsbad, CA, USA) at 37°C for 60 min. Nuclei were counterstained with 4',6-diamidino-2-phenylindole (DAPI; 1:500, Invitrogen) for 30 s. After washing three times, cells were imaged under a fluorescence microscope (Olympus, Japan) and counted and processed using Image-Pro Plus (IPP) 6.0 software (Media Cybernetics, America).

*Tissue samples:* After tissue perfusion and separation, samples were fixed with 4% paraformaldehyde in a 10% sucrose solution for 2 h, and then immersed in 30% sucrose solution at 4°C overnight. Tissues were embedded in optimal cutting temperature compounds (OCT) and sections (thickness, 10 μm) were prepared using a cryostat-microtome (Thermo Shandon, Cheshire, UK).

*Regenerated nerve staining*

Six months after surgery, eight mice were randomly sampled from each group for regenerated nerve staining. The protocols for nerve staining were the same as those used for cell sample staining. The primary antibodies were rabbit anti-MBP (1:50; Abcam), anti-S100 (1:500; Dako), anti-NF-H (1:200; Millipore, Boston, USA) and images were captured with a laser scanning confocal microscope (Leica, Germany).

*Adipose tissue double-staining*

The slides were rinsed with PBS to wash off OCT and then blocked with 10% goat serum for 30 min at 37°C. The slides were then incubated with rabbit anti-$P75^{NTR}$, anti-MBP and anti-Sox10 at 37°C for 2 h, followed by incubation with mouse anti-tubulinβ3 (1:200; Millipore) at 4°C overnight. Next day, after washing with PBS, slides were incubated with Alexa Fluor 488 goat anti-rabbit IgG (1:500; Invitrogen) and Alexa Fluor 555 goat anti-mouse IgG (1:500; Invitrogen) at 37°C for 45 min. Cell nuclei were counterstained with DAPI for 30 s. All sections were routinely stained with H&E and imaged using a microscope (Leica, Germany).

*Real-time RT-PCR analysis*

After 48 h of cultivation, cells were lysed with 1 ml Trizol (Invitrogen) and then washed with PBS and transferred to 1.5 ml Eppendorf tubes. After adding 400 μl chloroform, the solution was vigorously mixed for 30 s, placed on the ice for 15 min, and centrifuged at 12 000 rpm for 15 min at 4°C. The upper layer (clear, colorless) was mixed thoroughly with an equal volume of isopropyl alcohol. After centrifugation at 12 000 rpm for 10 min at 4°C, the supernatant was removed and the sediment was washed with 75% alcohol before centrifugation at 7500 rpm for 15 min at 4°C. The concentration of RNA dissolved in 40 μl DEPC-treated water was measured by spectrophotometry. The purified RNA sample (2 μg) was reverse transcribed to cDNA using in a reaction system (TaKaRa) containing 4 μl Buffer, 1 μl dNTPs, 1 μl Oligo, 1 μl reverse transcriptase, 1 μl enzyme inhibitor, 12 μl RNA and $H_2O$. The PCR amplification conditions were as follows: 30°C for 10 min followed by 42°C for 60 min; the completed reaction was maintained at 4°C.

Real-time RT-PCR analysis was performed in reaction system (10 μl) consisting of 1 μl upstream primers, 1 μl downstream primers, 1 μl cDNA and 7 μl DEPC-treated water. The following primers were used: S100 (5'-GCT GAG CAA GAA AGA ACT GAA-3' and 5'-AGC CAC CAG CAC AAC ATA C-3'); $P75^{NTR}$ (5'-GGT GAT GGC AAC CTC TAC AGT-3' and 5'-CCT CGT GGG TAA AGG AGT CTA-3'); Sox10 (5'-AGA TCC AGT TCC GTG TCA ATA A-3' and 5'-GCG AGA AGA AGG CTA GGT G-3'); MBP (5'-AGA GTC CGA CGA GCT TCA GA-3' and 5'-CAG GTA CTT GGA TCG CTG TG-3'); NCAM (5'-GGG AGG ATG CTG TGA TTG TCT-3' and 5'-GCA GGT AGT TGT TGG ACA GGA C-3'); and GAPDH (5'-TCC CAC TCT TCC ACC TTC-3' and 5'-CTG TAG CCG TAT TCA TTG TC-3'). The reaction conditions were as follows: 95°C for 10 min, followed by 40 cycles of 95°C for 30 s, 60°c for 30 s and 72°C for 45 s. Reactions were performed using the StrataGene Mx-3000p (Agilent Technologies, USA).

*ELISA analysis*

Cell culture supernatants were collected after 48 h in culture and analyzed by ELISA to measure NGF and BDNF secretions. ELISA kits for mouse BDNF and NGF (Syd Labs, USA) were used according to the manufacturer's instructions.

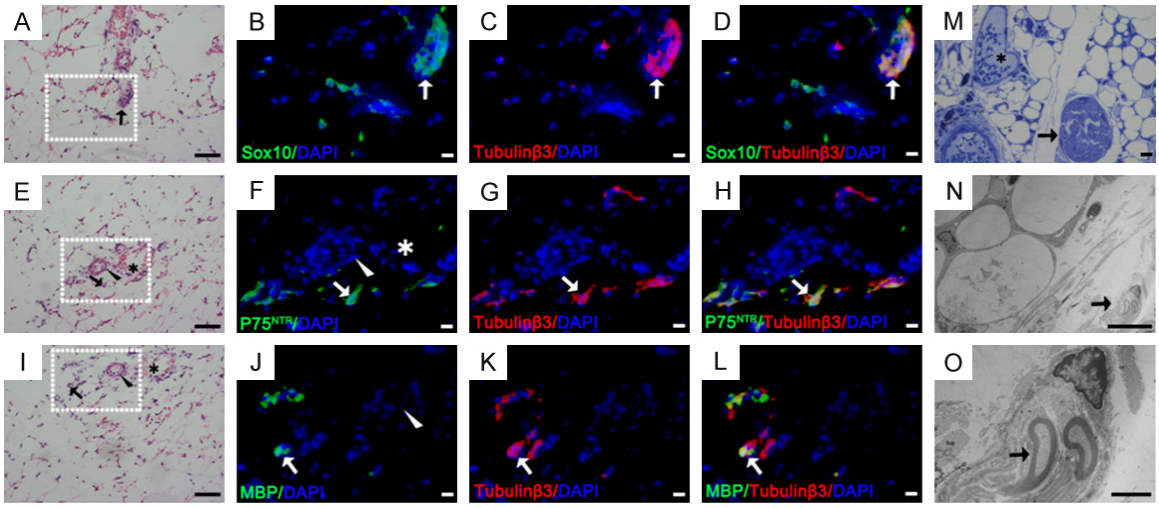


**Figure 1.** Detection and location of nerve tissues in mouse inguinal adipose tissue. (A, E, I) H&E staining of inguinal adipose tissue in neonatal mice. SC markers (green) of Sox10 (B-D), $P75^{NTR}$ (F-H) and MBP (J-L) were double-stained (yellow, arrow) with anti-tubulinβ3 antibody (red) in the H&E stained area. (M-O) Toluidine blue staining and TEM of inguinal adipose tissue in mice. (O) Partial enlargement of figure (N) Arrowhead: arterioles; Asterisk: small veins; Arrow: nerve tissues and SCs. Blue: DAPI. Bar = 50 μm (H&E, M), bar = 10 μm (fluorescent images, N), bar = 2 μm (O).

*Animal experiment*

$EGFP^+$ SNSCs, SCLC-H, SCLC-M and SCLC-L were used as seed-cells to repair 3 mm sciatic nerve defects in WT mice (n = 8 per group). Identical surgical protocols were used for all mice. For each group, cells were trypsinized and suspended in Matrigel (BD Biosciences, Franklin Lakes, NJ, USA) and mixed with DMEM (1:1). The concentration was at least $1\times10^6$ cells per 100 μl mixed fluid. Cell suspensions were divided into 1.5 ml Eppendorf tubes and incubated on ice for subsequent experiments. All surgical procedures were performed using microsurgical instruments (Zhangjiagang Oscar Medical Instruments, Zhangjiagang, China) under an operating microscope (Leica, Germany). Mice were anesthetized via an intraperitoneal injection of 0.5% chloral hydrate (6 ml/kg). Right sciatic nerves were exposed and cut off to create 3 mm nerve defects. Silicone tubes (Shanghai Sincere Industry) were inserted into the nerve injury sites and sutured with 8-0 microsurgical sutures (Shanghai Pudong Jinhuan Medical Products). Next, 10 μl mixed fluid was slowly injected into the silicone tube via the anastomotic suture gap. Finally, muscle and skin incisions were sutured with 5-0 nylon sutures. Animals in each group were randomly sampled 6 months after surgery for histological examinations.

*Transmission electron microscopy*

Inguinal adipose tissues of 3 adult mice were fixed with 2% glutaraldehyde at 4°C for 2 h and washed twice with PBS. Tissues were fixed with 1% osmic acid (diluted with PBS) at 4°C for 2 h. After washing with PBS at 4°C for 10 min, tissues were dehydrated using agraded series of alcohol solutions in the following order: 30%-50%-70%, 80%-95%-100%-100% alcohol for 10 min each. Epoxypropane was used twice to replace alcohol for 10 min. Tissues were saturated with expoxy resins 618 and epoxypropane (1:1) for 2 h before being heated to 60°C for 48 h for embedding. Semi-thin sections (1 μm thickness) were cut using an LKB-V ultramicrotome (LKB ProdukterB, Stockholm; Sweden), stained with toluidine blue and photographed using an Axiocam digital camera (Zeiss, Oberkochen, Germany). Finally, samples were cut into ultra-thin sections (50 nm thickness), stained with lead citrate and observed under a CM-120 transmission electron microscope (Philips, Netherlands).

*Statistical analysis*

All data are reported as means ± standard deviations (SD). All statistical analyses were performed using the statistical software SPSS version 19.0 (SPSS, Chicago, IL, USA). Paired t-tests were used to compare differences between two groups. Differences between

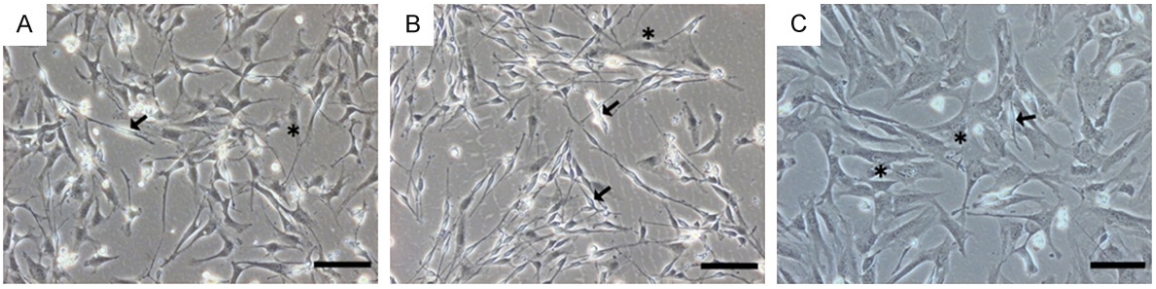


**Figure 2.** P0 and P2 adipose-derived cells. (A) Adipose-derived primary cells cultured for 24 h in vitro. SCLCs were bipolar or tripolar with strong refraction (arrow), and FLCs were large, flat and poorly refractive (asterisk). The number of P2 SCLCs (B) and FLCs (C) markedly increased through two rounds of purification. Bar = 100 μm.

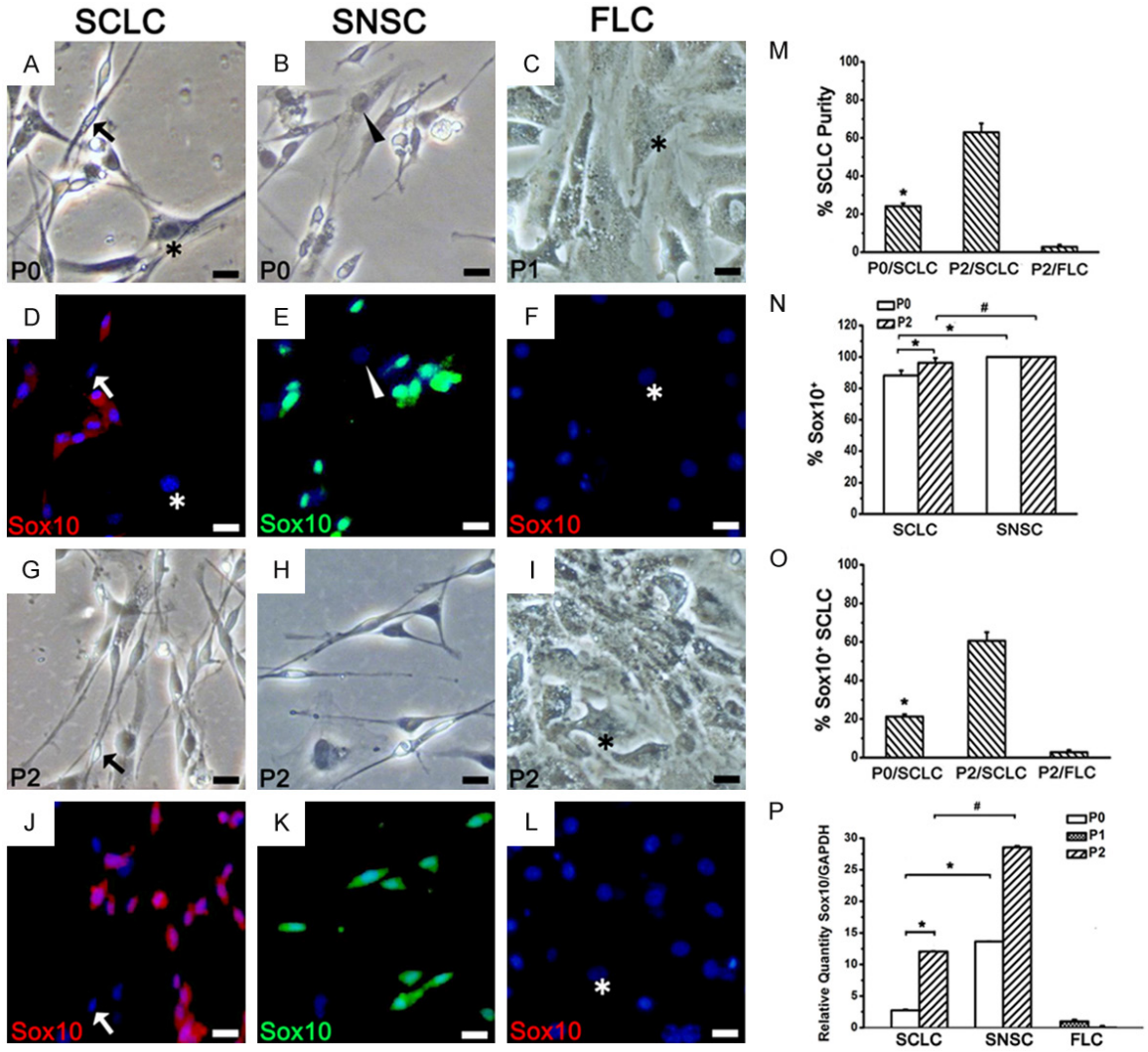


**Figure 3.** Phenotypic identification of SCLC by Sox10 immunofluorescent staining. (A-C, G-I) Bright field view of SCLCs, SNSCs in P0 and P2 and FLCs in P1 and P2. (D-F, J-L) Sox10 staining of (A-C) and (G-I) Blue: DAPI. In P2, a few SCLCs were $Sox10^-$ (J, arrow), while all SNSCs stably expressed Sox10 (E, K). All FLCs (asterisk) and fibroblasts (arrowhead) were $Sox10^-$. (M) SCLC purity in P0 and P2 adipose-derived total adherent cells. (N) Percentage of $Sox10^+$ cells in P0 and P2 total spindle-shaped cells. (O) Percentage of $Sox10^+$ SCLC (i.e. SC purity) in P0 and P2 total adherent cells. (P) The mRNA expression levels of Sox10 were detected using real-time RT-PCR in the three groups. $^*P < 0.05$, $^\#P < 0.05$. Bar = 20 μm.

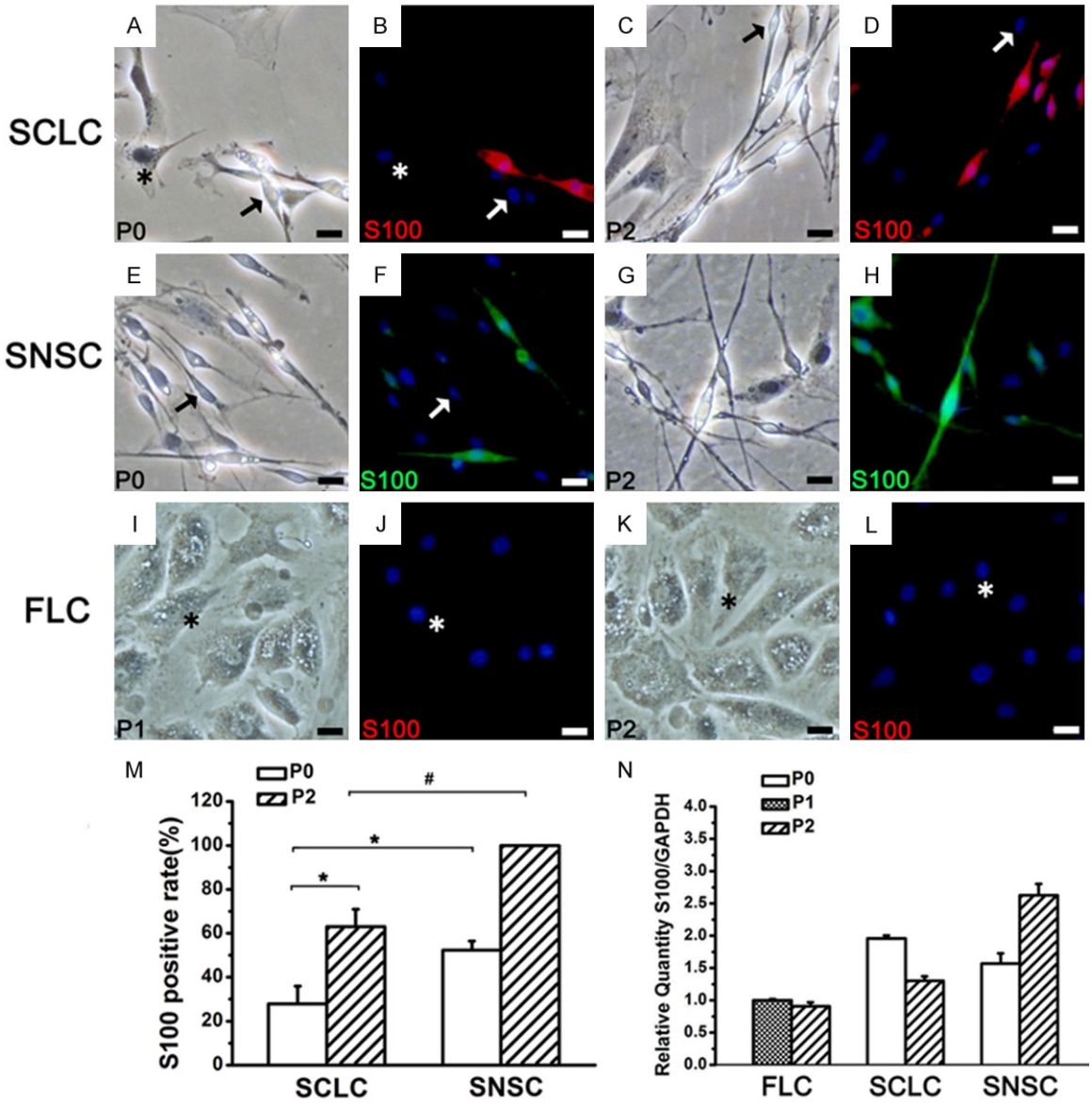


**Figure 4.** The expression of S100 in SCLC, SNSC and FLC. In P0, some SCLCs and SNSCs were S100$^-$ (A, B, E, F arrow). In P2, a part of SCLCs were still S100$^-$ (C, D arrow), while all SNSCs expressed S100 (G, H). All FLCs (asterisk) were negative. P1 and P2 FLCs from adipose tissue were S100- (I-L). Blue: DAPI. (M) The percentage of S100$^+$ in SCLC and SNSC. (N) The mRNA expression levels of S100 in the three groups. *P < 0.01, #P < 0.01. Bar = 20 μm.

three or more groups were analyzed with one-way analysis of variance (ANOVA), followed by Tukey's post-hoc tests. Non-parametric tests (Kruskal-Wallis Test) were used when the variance was heterogeneous. P < 0.05 was considered to indicate statistical significance.

## Results

### *Detection and location of nerve tissue in adipose tissue*

To investigate the existence of nerve fibers and SCs in adipose tissue, we performed H&E staining, IF staining and TEM of inguinal adipose tissue. H&E staining showed that some structures looked similar to nerve fibers in adipose tissue (**Figure 1A**, **1E**, **1I**). Some were scattered individually in the tissue, however, most cells were located around small blood vessels (**Figure 1A**, **1E**, **1I**). Double-staining of the axonal marker Tubulinβ3 and the Schwann cell markers P75$^{NTR}$, MBP and Sox10 showed that the positive staining of three markers was adjacent to or overlapping the Tubulinβ3 staining (**Figure 1B-D**, **1F-H**, **1J-L**). Moreover, nerve fibers and SCs were observed through TEM (**Figure 1M-O**).

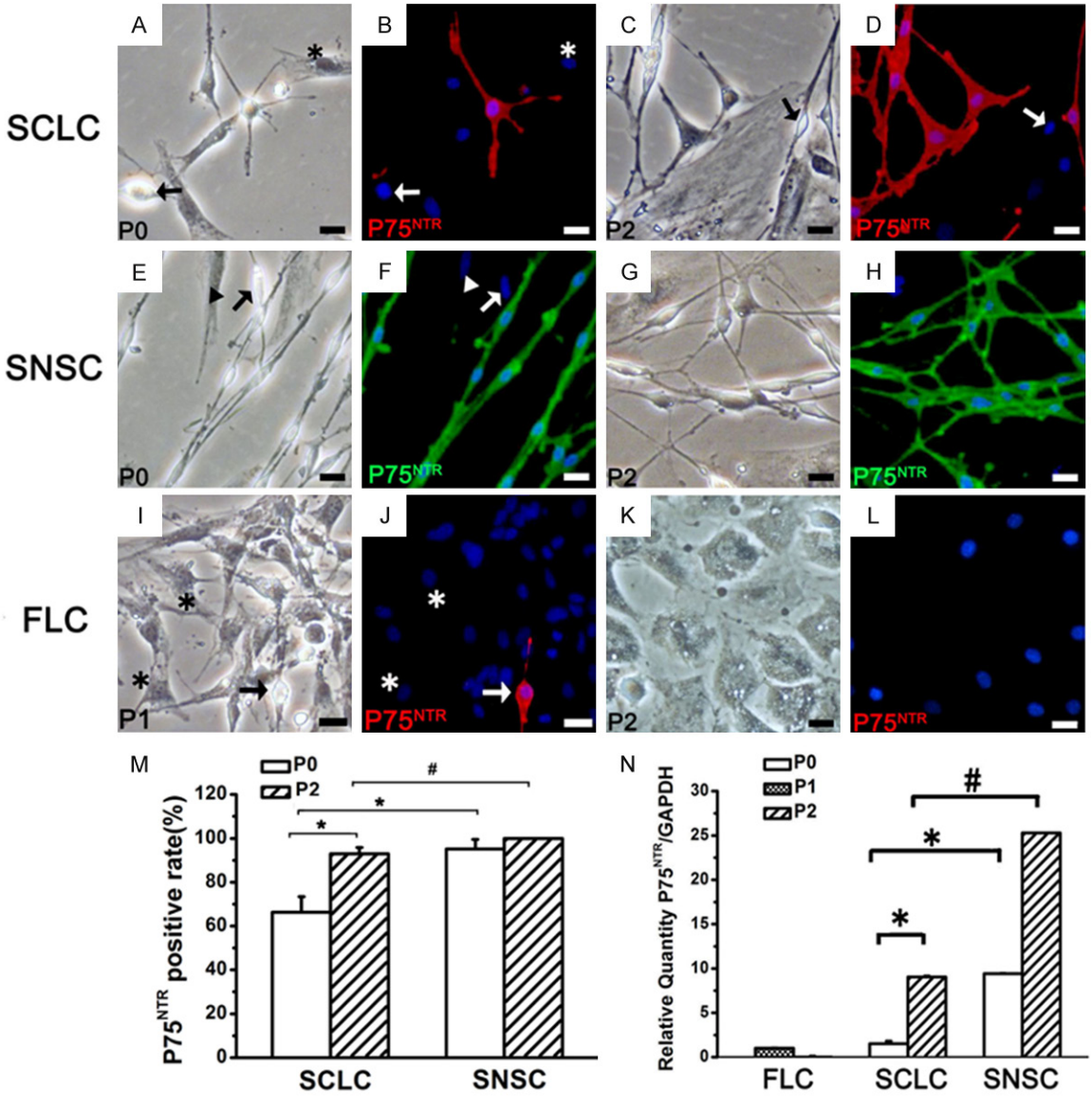


**Figure 5.** The expression of $P75^{NTR}$ in SCLC, SNSC and FLC. *P < 0.01, #P < 0.01. Bar = 20 μm.

These findings indicated the existence of SCs in adipose tissue.

*Cell isolation and enrichment from adipose tissue*

Cells were isolated from adipose tissue through enzymatic digestion. After 24 h in culture in vitro, adherent cells showed two main morphologies. Approximately 75% of all the cells were large, flat, irregular and poorly refractive (**Figure 2A**, asterisk) and were designated fibroblast-like cells (FLCs), while approximately 25% of the cells were bipolar or tripolar with strong refraction (**Figure 2A**, arrow) and were designated Schwann cell-like cells (SCLCs). In the primary culture, the purity of SCLCs was 24.1%±1.46% (**Figure 3M**). After two rounds of Dispase II digestion and enrichment, the purity increased to 63.0%±4.60%, and the purity of FLCs reached 97.2%±1.05% (**Figure 3M**).

*Phenotypic identification of SCLCs*

To determine the similarity between the phenotypes of SCLCs and SCs, we evaluated the expression of several SC markers such as Sox10 (**Figure 3**), S100 (**Figure 4**), $P75^{NTR}$ (**Figure 5**), NCAM (**Figure 6**) and MBP (**Figure 7**) in P0 and P2 SCLCs by IF staining. Sciatic

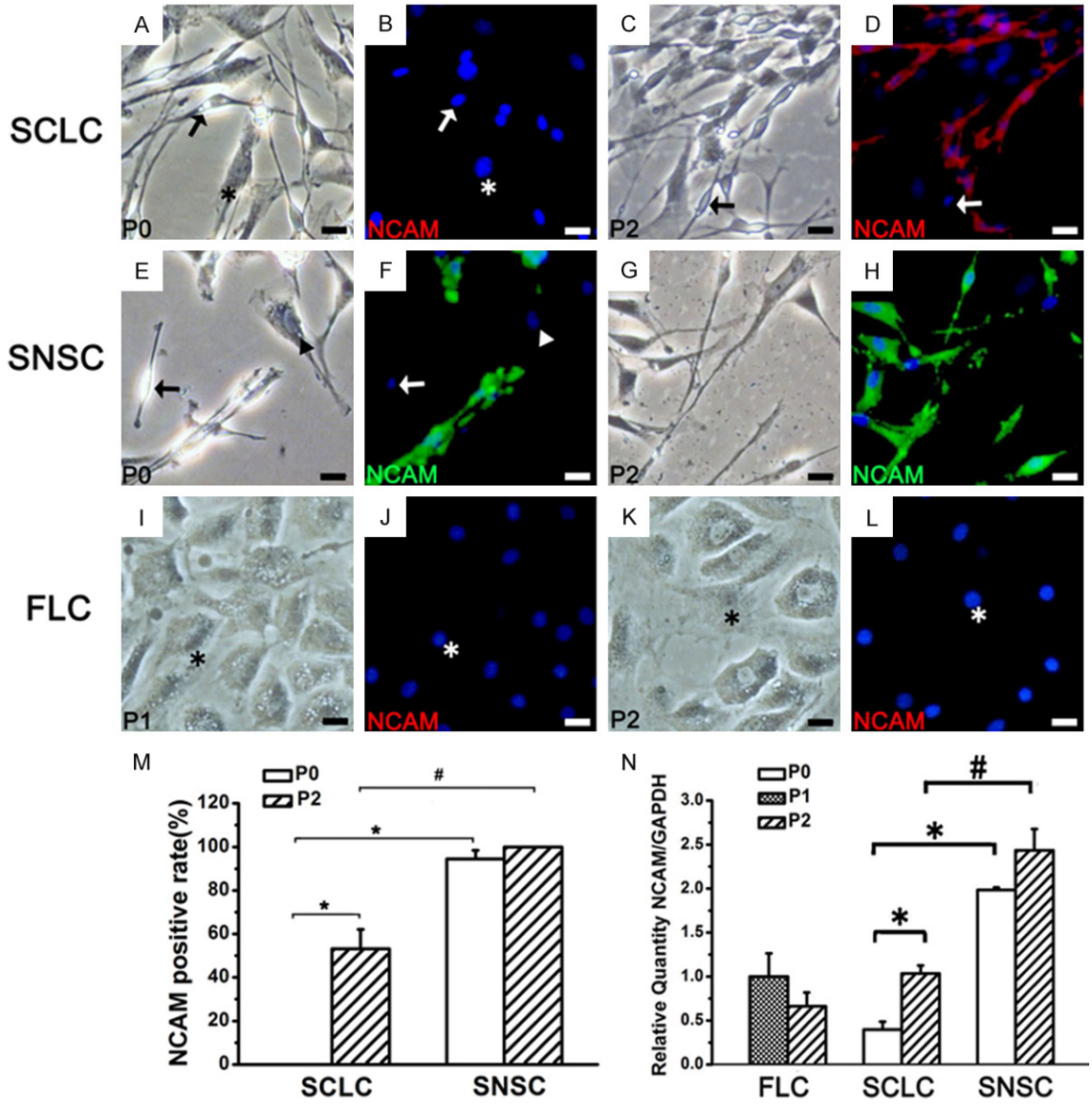


**Figure 6.** The expression of NCAM in SCLC, SNSC and FLC. *P < 0.01, #P < 0.01. Bar = 20 μm.

nerve-derived Schwann cells (SNSCs) and FLCs were used as positive and negative controls, respectively. We first observed the transcription factor Sox10, which is constitutively expressed in all neural crest-derived SCs [26, 27]. Sox10 is necessary for the development of neural crest cells into SCs, with an important role in Schwann cell differentiation and phenotypic stability [26-28]. The results showed that most SCLCs in P0 and P2 expressed Sox10 (**Figure 3D**, **3J**), while all FLCs were Sox10 negative (**Figure 3F**, **3L**). In P0 SCLCs, the percentage of Sox10$^+$ cells among the total population of spindle-shaped cells (not the total population of adherent cells) was 88.2%±3.12% (**Figure 3N** and **Table 1**) and increased to 96.2%± 3.06% in P2 (**Table 1**). However, the percentage of Sox10$^+$ cells among the SNSCs was consistently 100% (**Figure 3E**, **3K** and **Table 1**). Hence, in P0 SCLCs, P2 SCLCs, and P2 FLCs, the percentages of Sox10$^+$ SCLCs (i.e.SC purity) among all adherent cells was 21.2%±1.25%, 60.6%± 4.43% and 2.8%±1.05%, respectively (**Figure 3O**).

Further analysis of the expression of S100 (**Figure 4**) in the three groups showed that, unlike Sox10, S100 was not expressed in all P0

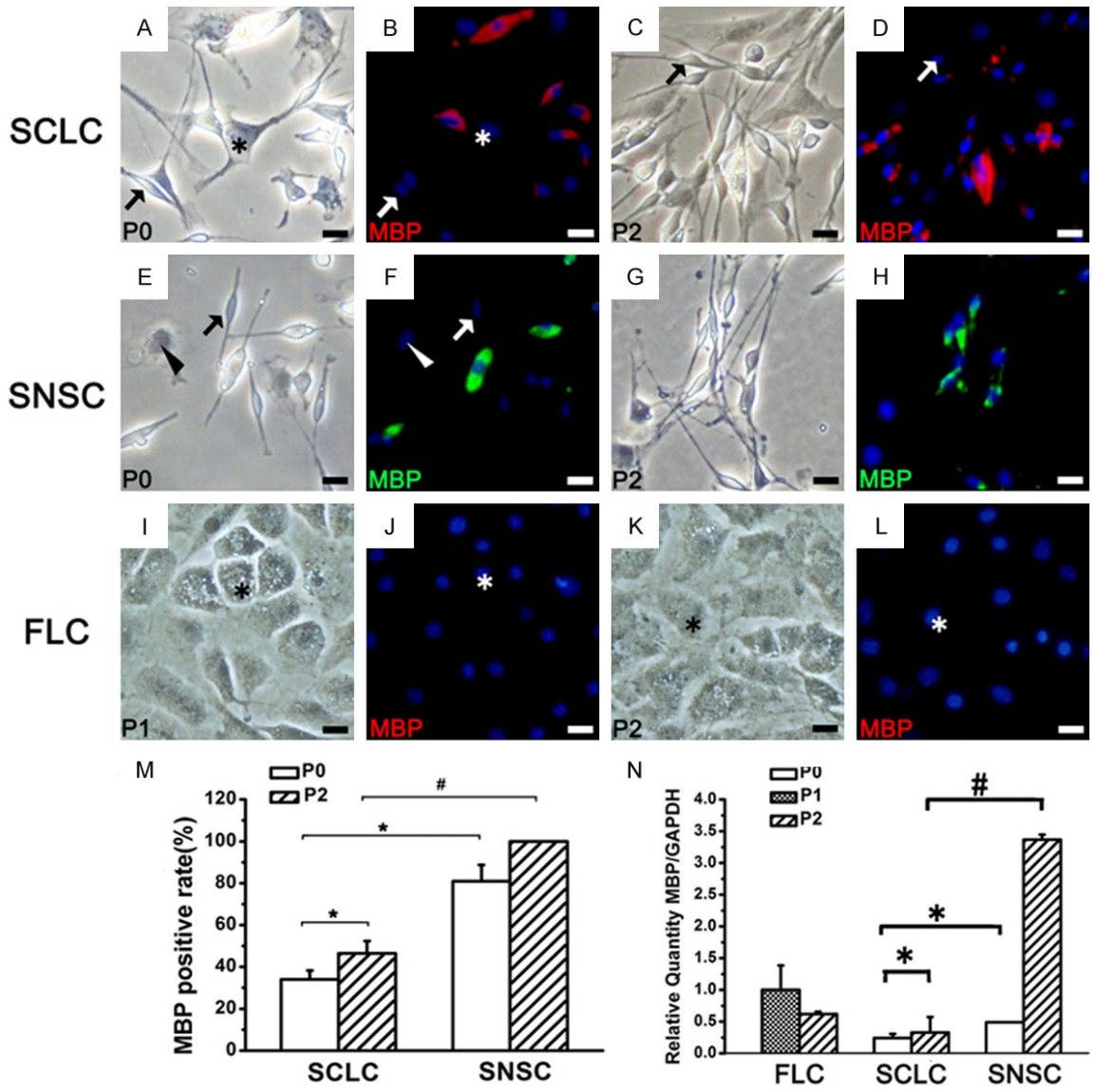


**Figure 7.** The expression of MBP in SCLC, SNSC and FLC. *P < 0.01, #P < 0.01. Bar = 20 μm.

**Table 1.** The percentage of SCLCs and SNSCs positive for SC markers (%)

| Markers | P0 SCLC | P2 SCLC | P0 SNSC | P2 SNSC |
|---|---|---|---|---|
| Sox10 | 88.2±3.12 | 96.2±3.06 | 100±0.00 | 100±0.00 |
| S100 | 27.8±8.08 | 63.0±8.02 | 52.3±4.08 | 100±0.00 |
| $P75^{NTR}$ | 66.3±7.16 | 93.0±2.77 | 95.2±4.38 | 100±0.00 |
| NCAM | 0.00±0.00 | 53.2±8.85 | 94.5±3.92 | 100±0.00 |
| MBP | 34.0±4.28 | 46.5±5.83 | 80.9±7.81 | 100±0.00 |

SNSCs and SCLCs and P2 SCLCs (**Table 1**). $P75^{NTR}$, NCAM and MBP exhibited the same pattern of expression (**Figures 5**-**7** and **Table 1**). The percentage of SCLCs and SNSCs positive for SC markers are summarized in **Table 1**.

Moreover, FLCs were cultured with SCCM and stained with SC markers to detect the impact of SCCM on FLCs differentiation; however neither neurospheres (**Figures 2C**, **3F**, **3L**) nor positive staining of five markers (**Figures 4**-**7I**-**L**) existed in FLCs indicating that SCCM medium can't convert FLCs into Schwann cells in our experiment.

Real-time RT-PCR analysis of the expression of these five markers in SCLCs showed that with increasing SC purity, the mRNA expression levels of Sox10 (**Figure 3P**), $P75^{NTR}$, NCAM and MBP (**Figures 5**-**7N**) had also obviously

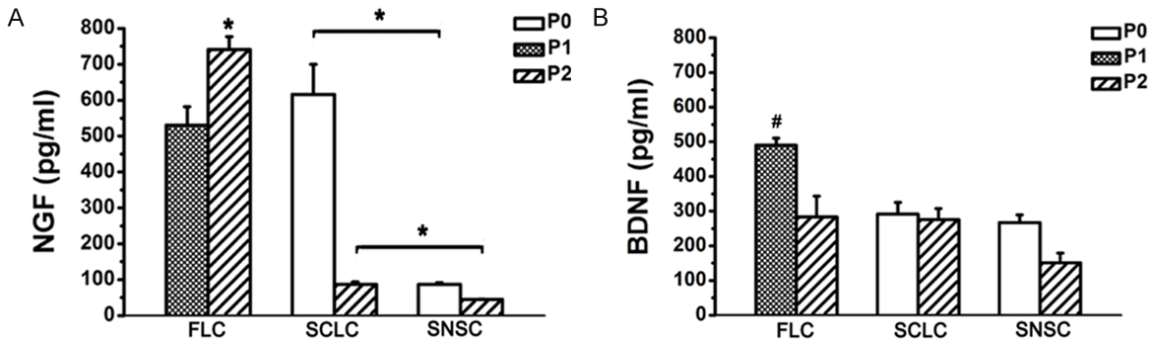


**Figure 8.** ELISA analysis of NGF and BDNF in SCLC, SNSC and FLC. The levels of NGF and BDNF secreted by FLCs were higher than those of the other two groups. *P < 0.01, #P < 0.01.

increased. A similar pattern of expression was observed in SNSCs, but the levels expressed in SCLCs were lower than those in SNSCs. These changes were consistent with those observed in IF staining; however, the mRNA expression levels of S100 in SCLCs apparently decreased with increasing culture time (**Figure 4N**).

*SCLC neurotrophic factor secretion*

We evaluated the neurotrophic factors by ELISA analysis of NGF and BDNF in supernatants of cultured SCLCs and SNSCs. FLC culture supernatants were used as a control. The ELISA results showed SCLCs could also secrete NGF (**Figure 8A**) and BDNF (**Figure 8B**). The levels of NGF secreted by P0 and P2 SCLCs were 616.1±83.34 pg/ml and 86.8±7.33 pg/ml, respectively, which were significantly higher than the levels secreted by P0 and P2 SNSCs (86.8±4.40 pg/ml and 45.1±0.72 pg/ml, respectively). The levels of BDNF secreted by P0 and P2SCLCs were 291.4±34.01 pg/ml and 275.9±31.70 pg/ml, respectively, which were also higher than the levels secreted by P0 and P2 SNSCs (267.2±22.19 pg/ml and 151.0± 28.37 pg/ml, respectively). Furthermore, we found that the levels of NGF and BDNF secreted by FLCs were distinctly higher than those of the other two groups.

*SCLC function in sciatic nerve regeneration*

To evaluate the ability of SCLCs to wrap around axons and form myelin sheaths in vivo, we injected SCLCs from CAG-EGFP mice into artificial nerve conduits to repair 3 mm sciatic nerve defects in wild-type (C67BL/6J) mice. Since we were unable to achieve completely purity of SCLCs in vitro at present, we evaluated the ability of SLCLs at three different levels of purity: SCLC-L (Low, 2.8%±1.05%), SCLC-M (Medium, 21.2%±1.25%) and SCLC-H (High, 60.6%± 4.43%) to repair sciatic nerve defects. SNSCs (purity 93.4%±2.14%) were used as a positive control.

After 3 months, the regenerated nerves were filled with $GFP^+$ cells (**Figure 9A-L**). IF staining exhibited that GFP double-stained with MBP, S100, and NF-H were more common in SCLC-H and SNSC than in SCLC-M and SCLC-L (**Figure 9Q**).

After 6 months, through TEM (**Figure 10M-P**), we found that the four groups all formed slim regenerated myelin sheaths and perineurium-like structures wrapping around axons and myelin sheaths. Some demyelination phenomena could still be observed. IF staining showed that $GFP^+$ cells in the SNSC group formed cyclic MBP positive structures (**Figure 10D**) and wrapped around NF-H positive axons (**Figure 10L**). Similar results were obtained through S100 staining (**Figure 10H**). Percentages of $GFP^+$ cells double-stained with MBP, S100, and NF-H were 87.9%±1.31%, 88.9%±1.95%, and 88.3%±1.47%, respectively (**Figure 10Q**). However, in the SCLC-L group, most $GFP^+$ cells formed irregular perineurium-like structures, wrapped around several $MBP^+$ SCs (**Figure 10A**) and $S100^+$ SCs (**Figure 10E**) and $NF\text{-}H^+$ axons (**Figure 10I**), with only a negligible number of $GFP^+$ cells expressing S100 and MBP. Percentages of $GFP^+$ cells double-stained with MBP, S100 and NF-H in this group were 0.7%±0.67%, 0.9%±0.95% and 1%±0.18%, respectively (**Figure 10Q**).

In the SCLC-M group, we also found abundant $GFP^+$ perineurium-like structures. At the same

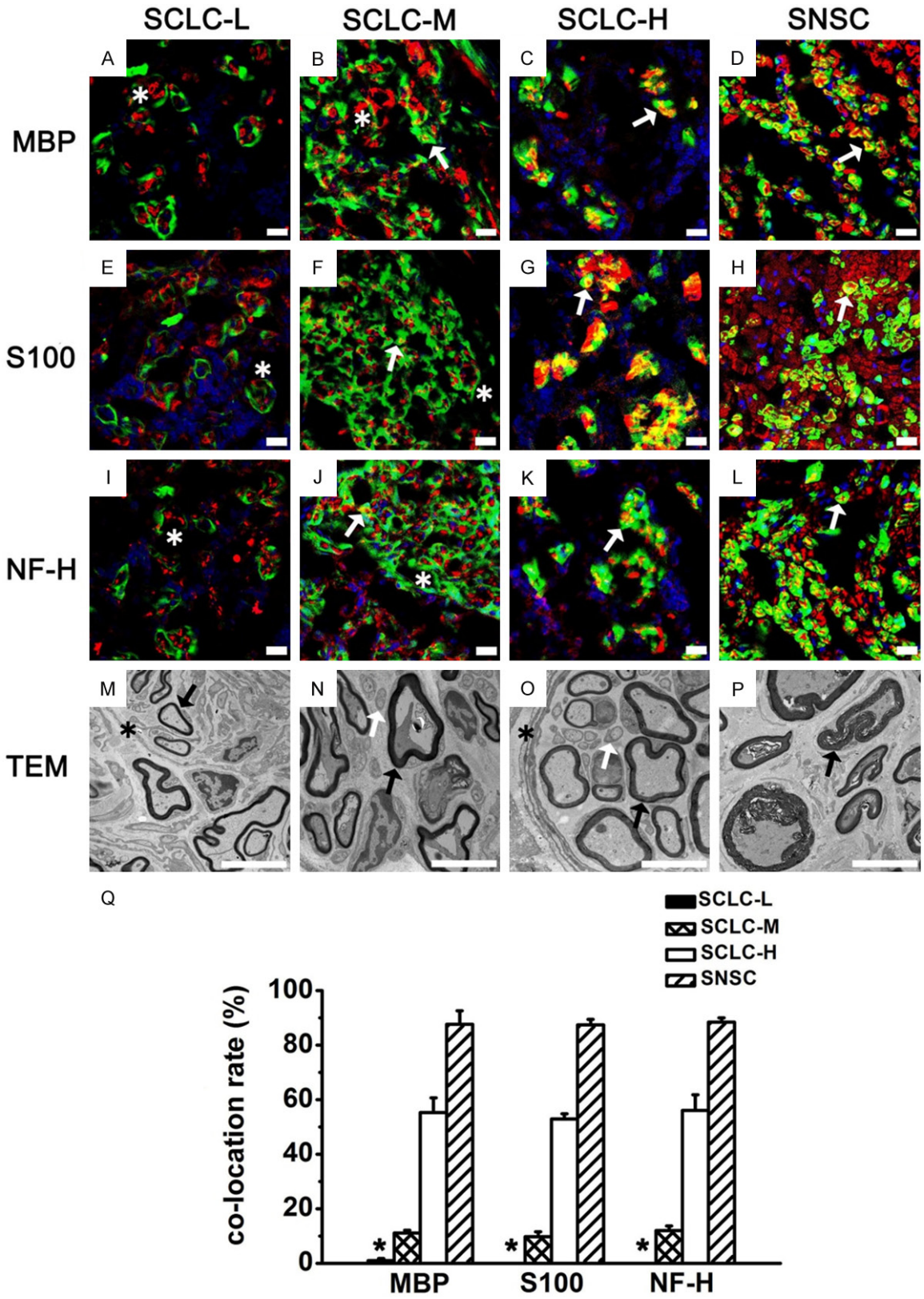


**Figure 9.** Regenerated sciatic nerves 3 months after surgery in the four groups. MBP (A-D, red), S100 (E-H, red), and NF-H (I-L, red) staining of regenerated sciatic nerves in the SCLC-L, SCLC-M, SCLC-H and SNSC group. Green: GFP. Red: MBP, S100, and NF-H. Yellow: co-located site. Blue: DAPI. M-P: Perineurium-like structures (asterisk), unmyelinated Schwann cells (white arrow), and myelinated Schwann cells (black arrow) were found in regenerated sciatic nerves by TEM. Q: Percentage of $GFP^+$ cells co-located with MBP, S100, and NF-H. *$P < 0.001$. Bar = 5 μm.

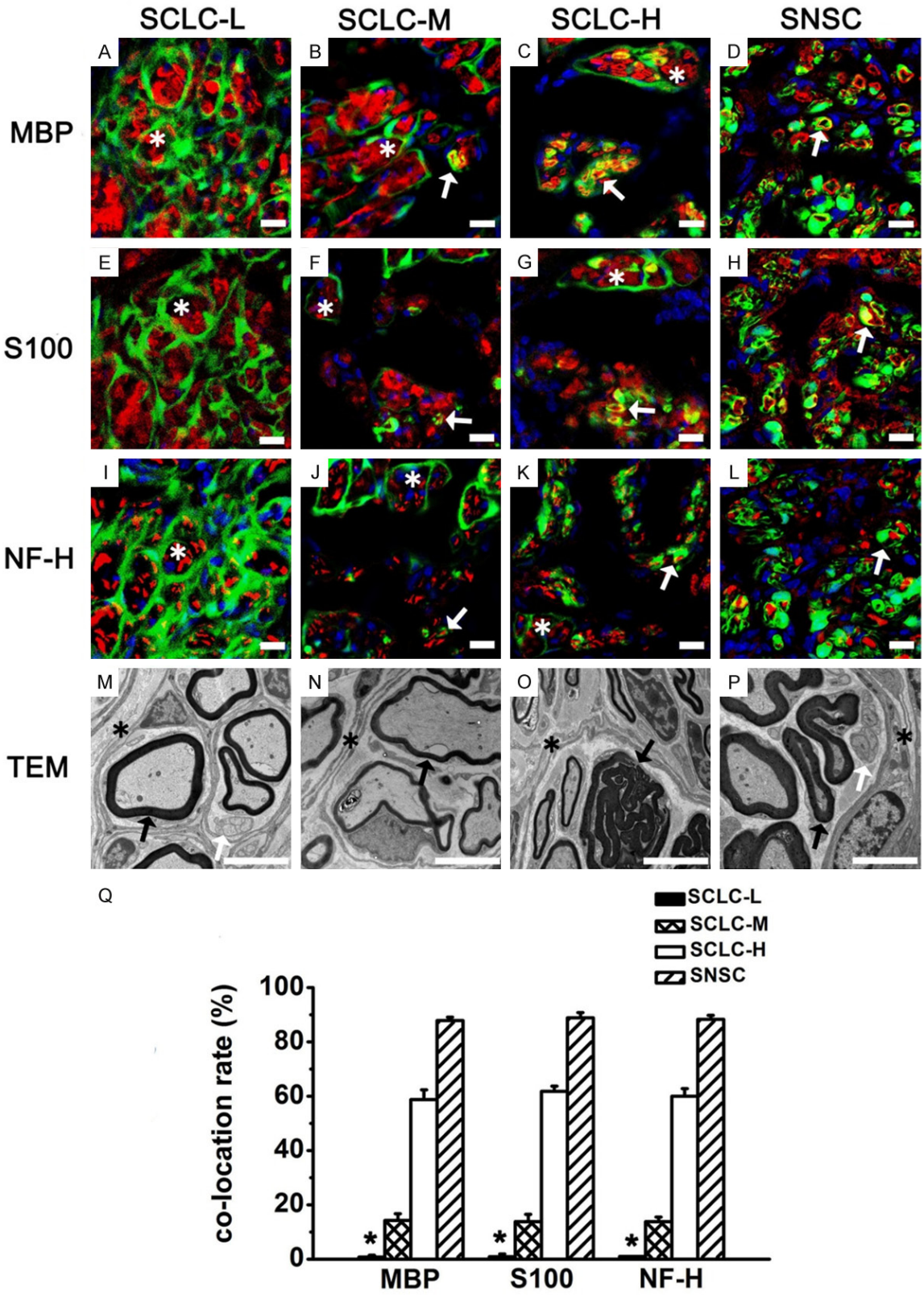


**Figure 10.** Regenerated sciatic nerves 6 months after surgery in the four groups. MBP (A-D, red), S100 (E-H, red), and NF-H (I-L, red) staining of regenerated sciatic nerves in the SCLC-L, SCLC-M, SCLC-H and SNSC. Green: GFP. Yellow: co-located site. Blue: DAPI. (M-P) Perineurium-like structures (asterisk), unmyelinated Schwann cells (white arrow), and myelinated Schwann cells (black arrow) were found in regenerated sciatic nerves by TEM. (Q) Percentage of $GFP^+$ cells co-located with MBP, S100, and NF-H. *$P < 0.001$. Bar = 5 μm.

time, we found a small number of $GFP^+$ cells forming $MBP^+$ cyclic structures (**Figure 10B**) and wrapping around a single NF-$H^+$ axon (**Figure 10J**). The results of S100 staining were similar to those of MBP staining. Percentages of $GFP^+$ cells double-stained with MBP, S100, and NF-H in the SCLC-M group were 14.3%± 2.45%, 13.8%±2.69%, and 13.8%±1.77%, respectively (**Figure 10Q**); however, in the SCLC-H group, a relatively high number of $GFP^+$, $MBP^+$ and $S100^+$ cells formed myelin sheaths and wrapped around axons (NF-$H^+$) (**Figure 10C**, **10G**, **10K**). In this group, percentages of $GFP^+$ cells double-stained with MBP, S100, and NF-H were 58.8%±3.61%, 61.8%±1.91%, and 60.0%±2.86%, respectively (**Figure 10Q**).

The four groups indicated that increased $GFP^+$ purity significantly increased the percentages of $GFP^+$ cells double-stained with MBP, S100 and NF-H, and increased the number of $GFP^+$ myelin sheaths. However, the number of perineurium-like structures gradually decreased.

## Discussion

In this experiment, we successfully isolated and enriched SCs from mice inguinal adipose tissue and also found that most adipose-derived cells cultured in vitro were FLCs. FLCs, which grow rapidly and have strong proliferation capacity [29, 30], will limit Schwann cell cultivation and purification. In our study, we found that the optimal time to purify primary SCLCs was after 24 h in culture. Moreover, those SCLCs adjacent to FLCs not only grew rapidly but were also resistant to digestion, indicating that FLCs may secrete neurotrophic factors to promote cell growth and sufficient extracellular matrix components to promote Schwann cell adhesion [31, 32]. Therefore, it is difficult to obtain highly purified SCs with routine methods [24]. We also tried adding 10 μg/ml mitomycin C to inhibit the growth of FLCs; however, this treatment suppressed the growth of SCs more effectively (data not shown). At present, the limit of SCLC purification is up to 60% and further investigations are required to increase the purity closer to 100%.

Our study indicates that SCLCs are very similar to SNSCs in shape and also express SC-specific markers S100, $P75^{NTR}$, MBP, Sox10 and NCAM. There are significant differences in the expression levels of these markers between SCLCs and SNSCs. Many researchers have reported that adipose tissue is innervated by sympathetic nerve fiber, which are mainly wrapped with unmyelinated SCs [20-22], while sciatic nerves are mixed nerves predominantly containing myelinated SCs. Therefore, we speculated that differences in the expression levels of SC markers between SCLCs and SNSCs may be due to different nerve type sources. In our study, we also found that Sox10 was not expressed in all SCLCs (**Figure 3D**, **3J**). It can be speculated that this difference is caused by the fact that some other adipose-derived cells are morphologically similar to SCs, as many researchers have demonstrated that all SCs are Sox10 positive [26, 27]. In this study, only $Sox10^+$ SCLCs were classified as SCs. Additionally, the expression levels of the cell differentiation markers, $P75^{NTR}$ and NCAM had increased with extended culture-time, indicating that SCLCs and SNSCs were gradually changing to a dedifferentiated state overtime in vitro.

In the SCLC-L group (SC purity, 2.8%±1.05%), very few $GFP^+$ cells were positive for S100 and MBP. One reason for this may be that very few Schwann cells in the SCLC-L group were positive for S100 and MBP. Alternatively, this could be attributed to the very few FLCs which were induced into SCs in vivo. The latter explanation is less likely based on the reports of Carlsonet al [31] and Silvia et al [33] that adipose-derived stem cells did not transform into SCs or neurons when they were used to repair peripheral nerve injuries. Furthermore, we speculate the role of adipose-derived stem cells is mediated not by direct contact with the axons of the sciatic nerve or transdifferentiation into SCs, but by secretion of growth factors, cytokines, and extracellular matrix components to promote new blood vessel formation and nerve regeneration just as reported by Carriel et al and Egles et al [34-36].

Many studies [37, 38] have shown that when nerves are damaged, the integrity of perineurium is destroyed, and fibroblasts wrap around several regenerated axons to form numerous perineurium-like structures that are distinctive from the actual perineuriums. Some researchers believe that these perineurium-like structures are mainly protective structures that protect regenerated nerves and reconstructed blood vessel-nerve barriers when repairing nerve injuries [39]. Interestingly, in our experi-

ments, FLCs transplanted into the injury sites also formed many perineurium-like structures, and these structures still existed in regenerated nerves six months after surgery. Thus, we speculated that FLCs perform a function similar to that of fibroblasts. Recently, some studies have shown that fibroblasts promote aggregation and directional migration of SCs in vitro and can enter the defective site ahead of SCs to guide Schwann cell migration in vivo [40]. Further studies are required to determine whether FLCs can perform similar function. By comparing different groups of SCLCs in vivo, we found that an increase in the purity of $GFP^+$ SCLCs also increased the amounts of $GFP^+$ myelin sheaths. With the increasing purity of $GFP^+$ FLCs, the amounts of $GFP^+$ perineurium-like structures also increased. Thus, we concluded that SCLCs have the ability to wrap around nerve axons and exert SCs function when they are used to repair nerve injuries in vivo.

In conclusion, Mouse inguinal adipose tissue contains nerve fibers and SCs that can be extracted through enzyme digestion. These cell phenotypes are slightly different from SNSCs in vitro, but in vivo they have the ability to form myelin sheaths in the same way as SNSCs.

## Acknowledgements

This work was supported by the National Natural Science Foundation (No. 31170932, No. 81000522 and No. 81671908), Capital Characteristic Key Project of Beijing Municipal Science and Technology Commission (No. z141107002514007). We thank Shanghai Key Laboratory of Tissue Engineering for their technical support.

## Disclosure of conflict of interest

None.

**Address correspondence to:** Dr. Zuoliang Qi, Department No. 16 of Plastic Surgery Hospital, Chinese Academy of Medical Sciences & Peking Union Medical College, 33 Badachu Rd, Shijingshan District, Beijing 100144, PR China. Tel: +8610 88772233; Fax: +861088964137; E-mail: qizuoliianglh@163.com; Dr. Zunli Shen, Department of Plastic and Reconstructive Surgery, Shanghai 1st People's Hospital, Shanghai Jiao Tong University School of Medicine, 100 Hai-Ning Rd, Shanghai 200080, PR China. Tel: +8621 63240090; Fax: +8621 63240825; E-mail: zunlishen@163.com

## References

[1] Radtke CV, Peter M. Peripheral nerve regeneration A current perspective. Eplasty 2009; 9: e47.

[2] Hadlock T, Sundback C, Hunter D, Cheney M and Vacanti JP. A polymer foam conduit seeded with Schwann cells promotes guided peripheral nerve regeneration. Tissue Eng 2000; 6: 119-127.

[3] Meyer M, Matsuoka I, Wetmore C, Olson L and Thoenen H. Enhanced synthesis of brain-derived neurotrophic factor in the lesioned peripheral nerve: different mechanisms are responsible for the regulation of BDNF and NGF mRNA. J Cell Biol 1992; 119: 45-54.

[4] Friedman B, Scherer SS, Rudge JS, Helgren M, Morrisey D, McClain J, Wang DY, Wiegand SJ, Furth ME, Lindsay RM and et al. Regulation of ciliary neurotrophic factor expression in myelin-related Schwann cells in vivo. Neuron 1992; 9: 295-305.

[5] Raivich G and Makwana M. The making of successful axonal regeneration: genes, molecules and signal transduction pathways. Brain Res Rev 2007; 53: 287-311.

[6] Keilhoff G, Pratsch F, Wolf G and Fansa H. Bridging extra large defects of peripheral nerves: possibilities and limitations of alternative biological grafts from acellular muscle and Schwann cells. Tissue Eng 2005; 11: 1004-1014.

[7] Nishiura Y, Brandt J, Nilsson A, Kanje M and Dahlin LB. Addition of cultured Schwann cells to tendon autografts and freeze-thawed muscle grafts improves peripheral nerve regeneration. Tissue Eng 2004; 10: 157-164.

[8] Wakao S, Hayashi T, Kitada M, Kohama M, Matsue D, Teramoto N, Ose T, Itokazu Y, Koshino K, Watabe H, Iida H, Takamoto T, Tabata Y and Dezawa M. Long-term observation of auto-cell transplantation in non-human primate reveals safety and efficiency of bone marrow stromal cell-derived Schwann cells in peripheral nerve regeneration. Exp Neurol 2010; 223: 537-547.

[9] Amoh Y, Hamada Y, Aki R, Kawahara K, Hoffman RM and Katsuoka K. Direct transplantation of uncultured hair-follicle pluripotent stem (hfPS) cells promotes the recovery of peripheral nerve injury. J Cell Biochem 2010; 110: 272-277.

[10] Biernaskie J and Miller FD. White matter repair: skin-derived precursors as a source of myelinating cells. Can J Neurol Sci 2010; 37 Suppl 2: S34-41.

[11] Walsh S, Biernaskie J, Kemp SW and Midha R. Supplementation of acellular nerve grafts with skin derived precursor cells promotes periph-

eral nerve regeneration. Neuroscience 2009; 164: 1097-1107.
[12] Solders G. Discomfort after fascicular sural nerve biopsy. Acta Neurol Scand 1988; 77: 503-504.
[13] Neundorfer B, Grahmann F, Engelhardt A and Harte U. Postoperative effects and value of sural nerve biopsies: a retrospective study. Eur Neurol 1990; 30: 350-352.
[14] Song L and Tuan RS. Transdifferentiation potential of human mesenchymal stem cells derived from bone marrow. FASEB J 2004; 18: 980-982.
[15] Faroni A, Smith RJ, Lu L and Reid AJ. Human Schwann-like cells derived from adipose-derived mesenchymal stem cells rapidly de-differentiate in the absence of stimulating medium. Eur J Neurosci 2016; 43: 417-430.
[16] Thomson JA, Itskovitz-Eldor J, Shapiro SS, Waknitz MA, Swiergiel JJ, Marshall VS and Jones JM. Embryonic stem cell lines derived from human blastocysts. Science 1998; 282: 1145-1147.
[17] Trott SA, Rohrich RJ, Beran SJ, Kenkel JM, Adams WP Jr and Robinson JB Jr. Sensory changes after traditional and ultrasound-assisted liposuction using computer-assisted analysis. Plast Reconstr Surg 1999; 103: 2016-2025; discussion 2026-2018.
[18] Pitman GH and Teimourian B. Suction lipectomy: complications and results by survey. Plast Reconstr Surg 1985; 76: 65-72.
[19] Jahromy FZ, Behnam H, Mansoori K, Rahimi AA, Edalat R and Mobarake JI. The effect of ultrasound on the expression of CNTF gene, a possible cause of ultrasound influence on the rate of injured peripheral nerve regeneration. Australas Phys Eng Sci Med 2013; 36: 323-329.
[20] Bamshad M, Aoki VT, Adkison MG, Warren WS and Bartness TJ. Central nervous system origins of the sympathetic nervous system outflow to white adipose tissue. Am J Physiol 1998; 275: R291-299.
[21] Song CK, Schwartz GJ and Bartness TJ. Anterograde transneuronal viral tract tracing reveals central sensory circuits from white adipose tissue. Am J Physiol Regul Integr Comp Physiol 2009; 296: R501-511.
[22] Bowers RR, Festuccia WT, Song CK, Shi H, Migliorini RH and Bartness TJ. Sympathetic innervation of white adipose tissue and its regulation of fat cell number. Am J Physiol Regul Integr Comp Physiol 2004; 286: R1167-1175.
[23] Ruschke K, Ebelt H, Kloting N, Boettger T, Raum K, Bluher M and Braun T. Defective peripheral nerve development is linked to abnormal architecture and metabolic activity of adipose tissue in Nscl-2 mutant mice. PLoS One 2009; 4: e5516.
[24] Jin YQ, Liu W, Hong TH and Cao Y. Efficient Schwann cell purification by differential cell detachment using multiplex collagenase treatment. J Neurosci Methods 2008; 170: 140-148.
[25] Liu Z, Jin YQ, Chen L, Wang Y, Yang X, Cheng J, Wu W, Qi Z and Shen Z. Specific marker expression and cell state of Schwann cells during culture in vitro. PLoS One 2015; 10: e0123278.
[26] Jessen KR and Mirsky R. The origin and development of glial cells in peripheral nerves. Nat Rev Neurosci 2005; 6: 671-682.
[27] Finzsch M, Schreiner S, Kichko T, Reeh P, Tamm ER, Bosl MR, Meijer D and Wegner M. Sox10 is required for Schwann cell identity and progression beyond the immature Schwann cell stage. J Cell Biol 2010; 189: 701-712.
[28] Vogl MR, Reiprich S, Kuspert M, Kosian T, Schrewe H, Nave KA and Wegner M. Sox10 cooperates with the mediator subunit 12 during terminal differentiation of myelinating glia. J Neurosci 2013; 33: 6679-6690.
[29] Meirelles Lda S and Nardi NB. Murine marrow-derived mesenchymal stem cell: isolation, in vitro expansion, and characterization. Br J Haematol 2003; 123: 702-711.
[30] Mitchell JB, McIntosh K, Zvonic S, Garrett S, Floyd ZE, Kloster A, Di Halvorsen Y, Storms RW, Goh B, Kilroy G, Wu X and Gimble JM. Immunophenotype of human adipose-derived cells: temporal changes in stromal-associated and stem cell-associated markers. Stem Cells 2006; 24: 376-385.
[31] Carlson KB, Singh P, Feaster MM, Ramnarain A, Pavlides C, Chen ZL, Yu WM, Feltri ML and Strickland S. Mesenchymal stem cells facilitate axon sorting, myelination, and functional recovery in paralyzed mice deficient in Schwann cell-derived laminin. Glia 2011; 59: 267-277.
[32] Sowa Y, Imura T, Numajiri T, Nishino K and Fushiki S. Adipose-derived stem cells produce factors enhancing peripheral nerve regeneration: influence of age and anatomic site of origin. Stem Cells Dev 2012; 21: 1852-1862.
[33] Marconi S, Castiglione G, Turano E, Bissolotti G, Angiari S, Farinazzo A, Constantin G, Bedogni G, Bedogni A and Bonetti B. Human adipose-derived mesenchymal stem cells systemically injected promote peripheral nerve regeneration in the mouse model of sciatic crush. Tissue Eng Part A 2012; 18: 1264-1272.
[34] Carriel V, Garrido-Gomez J, Hernandez-Cortes P, Garzon I, Garcia-Garcia S, Saez-Moreno JA, Del Carmen Sanchez-Quevedo M, Campos A and Alaminos M. Combination of fibrin-agarose hydrogels and adipose-derived mesenchymal stem cells for peripheral nerve regeneration. J Neural Eng 2013; 10: 026022.

[35] Lopatina T, Kalinina N, Karagyaur M, Stambolsky D, Rubina K, Revischin A, Pavlova G, Parfyonova Y and Tkachuk V. Adipose-derived stem cells stimulate regeneration of peripheral nerves: BDNF secreted by these cells promotes nerve healing and axon growth de novo. PLoS One 2011; 6: e17899.

[36] Luo H, Zhang Y, Zhang Z and Jin Y. The protection of MSCs from apoptosis in nerve regeneration by TGFβ1 through reducing inflammation and promoting VEGF-dependent angiogenesis. Biomaterials 2012; 33: 4277-4287.

[37] Jurecka W, Ammerer HP and Lassmann H. Regeneration of a transected peripheral nerve. An autoradiographic and electron microscopic study. Acta Neuropathol 1975; 32: 299-312.

[38] Yamamoto M, Okui N, Tatebe M, Shinohara T and Hirata H. Regeneration of the perineurium after microsurgical resection examined with immunolabeling for tenascin-C and alpha smooth muscle actin. J Anat 2011; 218: 413-425.

[39] Ahmed AM and Weller RO. The blood-nerve barrier and reconstitution of the perineurium following nerve grafting. Neuropathol Appl Neurobiol 1979; 5: 469-483.

[40] Parrinello S, Napoli I, Ribeiro S, Wingfield Digby P, Fedorova M, Parkinson DB, Doddrell RD, Nakayama M, Adams RH and Lloyd AC. EphB signaling directs peripheral nerve regeneration through Sox2-dependent Schwann cell sorting. Cell 2010; 143: 145-155.